



Thermodynamic modeling and optimization of the Fe–Ni–Ti system

Jozefien De Keyzer^a, Gabriele Cacciamani^{b,*}, Nathalie Dupin^c, Patrick Wollants^a

^a Dept. Metaalkunde en Toegepaste Materiaalkunde (MTM), Faculty of Engineering Sciences, K.U.Leuven, Kasteelpark Arenberg 44, 3001 Leuven, Belgium

^b Dip. di Chimica e Chimica Industriale, Università di Genova, Via Dodecaneso 31, I-16146 Genova, Italy

^c Calculé Thermodynamique, 3 rue de l'Avenir, 63670 Orcet, France

ARTICLE INFO

Article history:

Received 23 May 2008

Received in revised form

5 October 2008

Accepted 6 October 2008

Available online 4 November 2008

Dedicated to the memory of Prof. Riccardo Ferro

Keywords:

CALPHAD

Fe–Ni–Ti

Thermodynamics of alloys

Phase equilibria

ABSTRACT

A thermodynamic assessment of the ternary Fe–Ni–Ti system together with a partial reassessment of the binary sub-systems Ni–Ti and Fe–Ti was made following the CALPHAD method and using the compound energy formalism (CEF). Two and four sublattices were used to model the bcc and fcc phases respectively. This allows describing the order–disorder transformations occurring not only in the ternary Fe–Ni–Ti system, but also in the quaternary Al–Fe–Ni–Ti system. The description of the C14 Laves phase $TiFe_2$ was modified to three sublattices in order to be consistent with other Al–Fe–Ni–Ti sub-systems in which a three sublattice model is needed.

Thermodynamic parameters were optimized using the available experimental data. On the basis of this optimization the stable phase diagram is calculated. Moreover stable and metastable equilibria between ordered and disordered phases based on fcc and bcc respectively are calculated.

© 2008 Elsevier Ltd. All rights reserved.

1. Introduction

Each component element of the Fe–Ni–Ti ternary system is the main component of a wide range of alloys, such as steels (e.g. maraging steels), Ni-based superalloys and high strength, low weight Ti alloys. Even if those alloys usually exist out of more than ten elements, the ternary Fe–Ni–Ti subsystem can form the basis of further modeling. More specific applications for the Fe–Ni–Ti system are shape memory alloys and hydrogen storage materials [1]. Moreover, Fe–Ni–Ti is a subsystem of the Al–Fe–Ni–Ti system which is the subject of the European project COST 535 “Thalu” (Thermodynamics of Alloyed Aluminides). Actually, the present Fe–Ni–Ti thermodynamic modeling and optimization have been performed in view of its use for the modeling of the Al–Fe–Ni–Ti quaternary system. This has particularly influenced the choice of the sublattice models of the phases.

The first experimental studies of phase equilibria in the Fe–Ni–Ti system were performed in 1938 by Vogel and Wallbaum [2] but even now the Fe–Ni–Ti phase diagram is not known in detail. A critical assessment of the Fe–Ni–Ti constitutional properties has been recently published by Cacciamani et al. [1]. To our knowledge no Fe–Ni–Ti thermodynamic assessment has been previously published.

2. Thermodynamic models

Following the CALPHAD method [3,4], phase diagrams are calculated based on a description of the Gibbs free energy G of all the phases competing for equilibrium. The Gibbs free energy G^φ for a phase φ can be expressed as:

$$G^\varphi = {}^{ref}G^\varphi + {}^{id}G^\varphi + {}^{ex}G^\varphi + {}^{mag}G^\varphi \quad (1)$$

where ${}^{ref}G^\varphi$ is the reference Gibbs energy, ${}^{id}G^\varphi$ is the ideal mixing contribution and ${}^{ex}G^\varphi$ is the excess Gibbs energy. The fourth term accounts for magnetic contribution to the Gibbs energy, when a magnetic ordering occurs. Its expression, originally proposed by Inden [5] and successively modified by Hillert and Jarl [6], is:

$${}^{mag}G^\varphi = RT \ln(\beta + 1)f(\tau)$$

where β is usually assumed equal to the Bohr magnetic moment per mole of atoms, τ is the ratio T/T_c (T_c = critical temperature for magnetic ordering), and $f(\tau)$ is a polynomial expression.

For ternary liquid and disordered solid solutions the different ${}^{ref}G^\varphi$, ${}^{id}G^\varphi$ and ${}^{ex}G^\varphi$ terms can be written as:

$$\begin{aligned} {}^{ref}G^\varphi &= \sum_i x_i G_i^\varphi(T) \\ {}^{id}G^\varphi &= RT \sum_i x_i \ln x_i \\ {}^{ex}G^\varphi &= {}^{ex2}G^\varphi + {}^{ex3}G^\varphi \end{aligned} \quad (2)$$

* Corresponding author. Tel.: +39 010 353 6130x6152; fax: +39 010 362 5051.

E-mail address: cacciamani@chimica.unige.it (G. Cacciamani).

where x_i is the mole fraction of component i and $G_i^\varphi(T)$ the Gibbs energy of the pure component i in the structure of the phase φ . Its temperature dependence is expressed as:

$$G - H^{SER} = A + BT + CT \ln T + DT^2 + ET^{-1} + FT^3 + IT^7 + JT^{-9} \quad (3)$$

with A, B, C, D, \dots empirical parameters that are evaluated on the basis of the experimental information. Several temperature ranges with different expressions of this type can actually be needed.

Binary and ternary interaction terms in the excess Gibbs energy are expressed as:

$$\begin{aligned} ex^2 G^\varphi &= \sum_{i=1}^{n-1} \sum_{j=i+1}^n x_i x_j \sum_v v L_{i,j}^\varphi(T) (x_i - x_j)^v \\ ex^3 G_{A,B,C}^\varphi &= \sum_{i=1}^{n-2} \sum_{j=i+1}^{n-1} \sum_{k=j+1}^n x_i x_j x_k (u_i L_i^\varphi(T) \\ &\quad + u_j L_j^\varphi(T) + u_k L_k^\varphi(T)) \end{aligned} \quad (4)$$

with

$$u_i = x_i + \frac{1 - x_i - x_j - x_k}{3}.$$

In these expressions $L_i^\varphi(T)$ may have a temperature dependence similar to $G_i^\varphi(T)$:

$$\begin{aligned} L_i^\varphi(T) &= A + BT + CT \ln T + DT^2 \\ &\quad + ET^{-1} + FT^3 + IT^7 + JT^{-9}. \end{aligned} \quad (5)$$

For the solid solutions an additional contribution is added when at least one of the elements considered is magnetic.

Intermetallic phases, such as NiTi_2 , Ni_3Ti , NiTi , FeTi , Fe_2Ti and FeNi_3 , are modeled using the Compound Energy Formalism (CEF) as described by Hillert [7]. The component elements are assumed to occupy and possibly mix in two or more sublattices related by a simple formula, e.g. $(A, B)_m(C, D)_n$ meaning that A and B mix on the first sublattice while C and D mix on the second one. In this case the Gibbs energy is expressed as a function of the site fractions $y_i^{(s)}$, the mole fractions of each component i in the sublattice s . Site fractions obey the conditions:

$$\begin{aligned} \sum_i y_i^{(s)} &= 1 \\ \sum_s n^{(s)} y_i^{(s)} &= x_i \\ \sum_s n^{(s)} (1 - y_{va}) &= x_i \end{aligned} \quad (6)$$

where $n^{(s)}$ are the stoichiometric coefficients relating the sublattices (m and n in the previously mentioned example). The Gibbs energy of such a phase is given by:

$$\begin{aligned} {}^{ref} G^\varphi &= \sum_i \sum_j \cdots \sum_k y_i^{(1)} y_j^{(2)} \cdots y_k^{(s)} G_{i;j;\dots;k}^\varphi \\ {}^{id} G^\varphi &= \frac{1}{\sum_s n^{(s)}} RT \sum_s \sum_i n^{(s)} y_i^{(s)} \ln y_i^{(s)} \\ ex^2 G^\varphi &= \sum_s \sum_i \sum_j y_i^{(s)} y_j^{(s)} \sum_{r \neq s} \sum_k y_k^{(r)} L_{i,j;\dots;k}^\varphi(T) + \cdots \end{aligned} \quad (7)$$

where $G_{i;j;\dots;k}^\varphi$ in ${}^{ref} G^\varphi$ are the Gibbs energies of all the stoichiometric compounds (either stable, metastable or unstable) formed when only one constituent is present on each sublattice. $L_{i,j;\dots;k}^\varphi(T)$ in $ex^2 G^\varphi$ are interaction parameters corresponding to the mixing of components i and j on the sublattice s while the other sublattices

are singly occupied. More terms can be added to $ex^2 G^\varphi$, corresponding to simultaneous mixing on two sublattices while the remaining sublattices are singly occupied. $ex^3 G^\varphi$ accounts for the possible interactions of three elements in a given sublattice.

In the case where two or more phases are related by an order-disorder transformation, the Gibbs energy of those phases can be written with one expression [8,9]:

$$G_m = G_m^{dis}(x_i) + \Delta G_m^{ord}(y_i^s) \quad (8)$$

where $G_m^{dis}(x_i)$ is the energy of the disordered state and is given by Eq. (2) while

$$\Delta G_m^{ord} = G_m^{sl}(y_i^s) - G_m^{sl}(y_i^s = x_i) \quad (9)$$

is the difference between two contributions expressed according to Eq. (7), first calculated using the actual site occupation of the phase and then using the phase composition as site fractions which correspond to a disordered state.

3. Fe–Ni–Ti solid phases

The structures of the phases, stable or metastable, considered for the Fe–Ni–Ti thermodynamic assessment are reported in Table 1. In the same table stability ranges of the stable phases and the CEF models adopted in this work are also given.

3.1. fcc phases: γ -(Fe, Ni) and Fe_3Ni

Both ordered and disordered fcc phases are present in the Fe–Ni–Ti system on the Fe–Ni side of the phase diagram. The disordered phase is modeled using the simplest form of a sublattice model where the elements mix on one sublattice.

At lower temperatures an ordered fcc phase FeNi_3 with L_1_2 structure is formed in the Fe–Ni subsystem. This is the only stable ordered fcc phase in the Fe–Ni–Ti system. However, ordered fcc phases are stable in the other binary and ternary subsystems of the quaternary Al–Fe–Ni–Ti, such as, for example, L_1_0 TiAl . To make a consistent extrapolation to the quaternary system possible, all three fcc ordered compounds should therefore be modeled, even if they are metastable. Because of their structural relation to the disordered fcc phase, FeNi_3 , FeNi and Fe_3Ni are modeled using a four sublattice model related to the one sublattice model of the disordered fcc phase according to Eqs. (8) and (9). The FeNi_3 compound will result when Ni is the main element on three out of four sublattices, with the same site fraction on all of them, while Fe is the main element on the fourth.

Thanks to their crystallographic equivalence the four sublattices are also thermodynamically equivalent, which means that groups of selected G must be equal to each other. A number of constraints such as:

$$\begin{aligned} G_{\text{Fe:Ni:Ni:Ni}}^{fcc} &= G_{\text{Ni:Fe:Ni:Ni}}^{fcc} = G_{\text{Ni:Ni:Fe:Ni}}^{fcc} = G_{\text{Ni:Ni:Ni:Fe}}^{fcc} \\ G_{\text{Fe:Fe:Ni:Ni}}^{fcc} &= G_{\text{Fe:Ni:Fe:Ni}}^{fcc} = G_{\text{Fe:Ni:Ni:Fe}}^{fcc} = G_{\text{Ni:Fe:Fe:Ni}}^{fcc} \\ &= G_{\text{Ni:Fe:Ni:Fe}}^{fcc} = G_{\text{Ni:Ni:Fe:Fe}}^{fcc} \end{aligned} \quad (10)$$

$G_{\text{Fe:Fe:Fe:Ni}}^{fcc} = G_{\text{Fe:Fe:Ni:Fe}}^{fcc} = G_{\text{Fe:Ni:Fe:Fe}}^{fcc} = G_{\text{Ni:Fe:Fe:Fe}}^{fcc}$ holds. Similar considerations bring to the introduction of similar constraints on the interaction parameters L :

$$\begin{aligned} L_{\text{Fe,Ni:Ni:Ni}}^{fcc} &= L_{\text{Ni:Fe,Ni:Ni:Ni}}^{fcc} = L_{\text{Ni:Ni:Fe,Ni:Ni}}^{fcc} = L_{\text{Ni:Ni:Ni:Fe,Ni}}^{fcc} = \cdots \\ L_{\text{Fe:Fe,Ni:Ni:Ni}}^{fcc} &= L_{\text{Fe:Fe,Ni:Ni:Ni}}^{fcc} = L_{\text{Fe:Ni:Fe,Ni:Ni}}^{fcc} = L_{\text{Fe:Ni:Ni:Fe,Ni}}^{fcc} = \cdots \\ \cdots \end{aligned} \quad (11)$$

These constraints considerably reduce the number of independent empirical parameters to be evaluated during optimization.

Table 1

Fe–Ni–Ti solid phases considered in this work: crystal structure data, temperature and composition ranges of stability, sublattice models.

Phase name	Pearson symbol–Prototype space group strukturbericht	Lattice parameters (nm)	Temperature range (°C)	Composition range	Database phase name and Sublattice model
γ -(Fe, Ni)	<i>cF4</i> –Cu	Pure Fe: $a = 0.36467$	Fe: 1394–912	Fe–Ni: Complete solubility	A1 (Fe, Ni, Ti) disordered part of FCC4
	<i>Fm-3m</i> A1	Pure Ni: $a = 0.35232$ $\text{Fe}_{50}\text{Ni}_{50}: a = 0.3575$ $\text{Fe}_{80}\text{Ti}_{20}: a = 0.294$ $\text{Ni}_{90.6}\text{Ti}_{9.4}: a = 0.35568$ $\text{Fe}_{31}\text{Ni}_{63}\text{Ti}_6: a = 0.3590$ at room T $\text{Fe}_{21}\text{Ni}_{63}\text{Ti}_6: a = 0.3652$ at 900 °C $\text{Fe}_{64.4}\text{Ni}_{29.6}\text{Ti}_{6.0}: a = 0.35939$ $\text{Fe}_{68.3}\text{Ni}_{26.9}\text{Ti}_{4.8}: a = 0.35913$ $\text{Fe}_{68.3}\text{Ni}_{30.4}\text{Ti}_{1.3}: a = 0.35890$ $\text{Fe}_{71.7}\text{Ni}_{27.4}\text{Ti}_{1.2}: a = 0.35837$	Ni: <1455	Fe–Ti: 0–0.8 at.% Ti (γ loop) Ni–Ti: 0–13.7 at.% Ti	
α -Fe, δ -Fe β -Ti	<i>cl2</i> –W	Pure Fe: $a = 0.28665$	Fe: 1538–1394 and <912	Fe–Ni: 0–3 at.% Ni at 1514 °C 0–5 at.% Ni at ~500 °C Fe–Ti: 0–10 at.% Ti 0–22 at.% Fe Ni–Ti: 0–10 at.% Ni	A2 (Fe, Ni, Ti) disordered part of BCC2
	<i>Im-3m</i>	Pure Ti: $a = 0.33065$	Ti: 1670–882		
	A2	$\text{Ni}_{9.5}\text{Ti}_{90.5}: a = 0.3224$			
α -Ti	<i>hP2</i> –Mg <i>P6₃/mmc</i> A3	Pure Ti: $a = 0.29506$ $c = 0.46825$	Ti: <882	Fe–Ti: < 0.04 at.% Fe Ni–Ti: < 0.2 at.% Ni	A3 (Fe, Ni, Ti)
FeNi ₃	<i>cP4</i> –AuCu ₃	$a = 0.35523$	<517	Fe–Ni: 63– ~ 85 at.% Ni	FCC4 (Fe, Ni, Ti) _{1/4} (Fe, Ni, Ti) _{1/4} (Fe, Ni, Ti) _{1/4} (Fe, Ni, Ti) _{1/4} disordered contribution from A1
	<i>Pm-3m</i> L1 ₂			Ti solubility. Not known	
Fe ₃ Ni	<i>cP4</i> –AuCu ₃ <i>Pm-3m</i> L1 ₂	–	Metastable	Metastable	
FeNi	<i>tP4</i> –AuCu <i>P4/mmm</i> L1 ₀	–	Metastable	Metastable	
(Fe, Ni)Ti	<i>cP2</i> –CsCl	$\text{Fe}_{50}\text{Ti}_{50}: a = 0.29789$	FeTi: <1317	Fe–Ti: 49.7–52.5 at.% Ti	BCC2 (Fe, Ni, Ti, Va) _{1/2} (Fe, Ni, Ti, Va) _{1/2} disordered contribution from A2
	<i>Pm-3m</i> B2	$\text{Fe}_{25.3}\text{Ni}_{14.7}\text{Ti}_{50}: a = 0.29818$ $\text{Fe}_{25.3}\text{Ni}_{24.7}\text{Ti}_{50}: a = 0.29891$ $\text{Fe}_{10.2}\text{Ni}_{39.8}\text{Ti}_{50}: a = 0.3000$ $\text{Ni}_{52}\text{Ti}_{48}: a = 0.3010$ $\text{Fe}_{25}\text{Ni}_{25}\text{Ti}_{50}: a = 0.2985$	NiTi: <1311	Ni–Ti: 43–50.5 at.% Ti Fe–Ni–Ti: Complete solubility between FeTi and NiTi	
Fe ₂ Ti (Laves phase)	<i>hP12</i> –MgZn ₂	$\text{Fe}_{66.7}\text{Ti}_{33.3}: a = 0.4785$	<1427	Fe–Ti: 27.6–35.2 at.% Ti	C14 (Fe, Ni, Ti) ₁ (Fe, Ni, Ti) _{3/2} (Fe, Ni, Ti) _{1/2}
	<i>P6₃/mmc</i> C14	$c = 0.7799$ $\text{Fe}_{33.9}\text{Ni}_{33.0}\text{Ti}_{33.1}: a = 0.4956$ $c = 0.8032$		Fe–Ni–Ti: 0–30 at.% Ni.	
Ni ₃ Ti	<i>hP16</i> –TiNi ₃ <i>P6₃/mmc</i> D0 ₂₄	$\text{Ni}_{75}\text{Ti}_{25}: a = 0.51088$ $c = 0.83187$ $\text{Fe}_4\text{Ni}_{7.1}\text{Ti}_{25}: a = 0.5103$ $c = 0.8320$	<1380	Ni–Ti: 20–25 at.% Ti Fe–Ni–Ti: 0–20 at.% Fe	NI3T1 (Fe, Ni, Ti) ₃ (Fe, Ni, Ti) ₁
NiT ₂	<i>cF96</i> –NiTi ₂ <i>Fd-3m</i> E9 ₃	$\text{NiTi}_2: a = 1.13193$ $\text{Fe}_{19}\text{Ni}_{27}\text{Ti}_{54}: a = 1.1338$ $a = 1.1324 – 1.1350$ at 0–26.7 at.% Fe	<984	Ni–Ti: 66–67 at.% Ti Fe–Ni–Ti: 0–30 at.% Fe.	NIT12 (Fe, Ni, Ti) ₂ (Fe, Ni, Ti) ₁

See for instance the work of Kussofsky et al. [9] for a detailed discussion of the relations and constraints between parameters in the four-sublattice modeling of the fcc ordered phases. Finally each sublattice may contain Ti, in order to account for Ti solubility in both ordered and disordered phases and in view of the application of the model to other systems.

3.2. bcc phases: α – δ -Fe, β -Ti and (Fe, Ni)Ti

A disordered bcc solid solution (A2) is present at both the Fe- and the Ti-corners (α – δ -Fe and β -Ti) and an ordered B2 phase extends at about 50 at.% Ti, connecting the isostructural FeTi and NiTi binary compounds. The simplest model to describe the B2

Table 2

Positions of the atoms in the Laves phases.

Phase	Wyckoff position	Ideal occupation (%)	Main element	Coordination
C15 cF24-MgCu ₂	16d	100	Fe or Ni	12 icosahedron
	8a	100	Ti	16: Frank-Kasper polyhedron
C14 hP12-MgZn ₂	2a	100	Fe or Ni	12 icosahedron
	6h	100	Fe or Ni	12 icosahedron
	4f	100	Ti	16: Frank-Kasper polyhedron
C36 hP24-MgNi ₂	4f	100	Fe or Ni	12 icosahedron
	6g	100	Fe or Ni	12 icosahedron
	6h	100	Fe or Ni	12 icosahedron
	4e	100	Ti	16: Frank-Kasper polyhedron
	4f	100	Ti	16: Frank-Kasper polyhedron

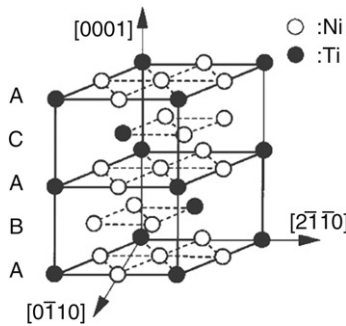


Fig. 1. Structure of the Ni₃Ti phase. Half of the atoms are sandwiched between layers of the same type (ABA stacking) and have hcp-type coordination, while the other half is sandwiched between layers of different type (ABC stacking) and have fcc-type coordination [12].

phase is a two-sublattice model where Ti is the main component on one sublattice and Fe and Ni mix as main components on the other one. From the crystallographic point of view, these sub-lattices can actually be switched keeping the resulting structure identical. This crystallographic equivalence imply a thermodynamic equivalence. The Gibbs energy of a stoichiometric compound AB in this structure is thus identical to the anti-structural one.

$$G_{A:B}^{B2} = G_{B:A}^{B2} \quad (12)$$

The same kind of relation stand also for interaction parameters.

$$L_{A,C:B}^{B2} = L_{B,A,C}^{B2} \quad (13)$$

These relations have in particular been described and discussed by Dupin et al. [10].

The fact that the B2 phase is an ordered state of the bcc structure allows in some systems (Al-Fe, Fe-Si) second order transitions between these phases. In order to describe this feature, their Gibbs energies need to be modeled with a single mathematical expression. This is performed thanks to Eqs. (8) and (9).

Moreover, vacancies are added in order to account for the triple defects identified in some binary B2 compounds. They have for instance been unambiguously evidenced in the Al-Ni system. To maintain symmetry between the sub-lattices and the possibility to describe the disordered state, the vacancies are introduced in both sublattices.

3.3. hcp phases: α -Ti

In the Ti-rich corner the hcp phase is stable in the form of α -Ti. Similar to the disordered fcc and bcc phases, the hcp phase is modeled using a single sub-lattice for the substitutional elements.

3.4. Laves phase: Fe₂Ti

In the Fe-Ni-Ti system, only C14 of the three main Laves phases is stable. Other Laves phases (C15 and C36) are metastable. Owing to the different number of crystallographic sublattices (2, 3 and 5 in C15, C14 and C36, respectively) all Laves phases have usually been modeled using 2 sublattices by collecting in the same sublattice the crystallographic sites with the same coordination polyhedron (see Table 2). In C14, however, three different Wyckoff positions may be distinguished and, in principle, three sublattices should be used. This should not be necessary for a satisfactory modeling of C14 in Fe-Ni-Ti, but in the Al-Ni-Ti ternary system the site occupancies determined by Grytsiv and coworkers [11] by Rietveld refinement on single crystals of this phase are significantly different for the two 12-coordinated sites. This behavior is associated with a bent shape of the C14 homogeneity range that could be very difficult to describe if only two sublattices are used. For this reason and in order to be consistent with crystallographic sublattices, the C14 Laves phase is then formally modeled as (Fe, Ni, Ti) (Fe, Ni, Ti)_{1.5}(Fe, Ni, Ti)_{0.5} instead of (Fe, Ni, Ti)(Fe, Ni, Ti)₂, but constraints between parameters make the description substantially equivalent to the two-sublattice description.

3.5. NiTi₂ and Ni₃Ti

The NiTi₂ phase shows a very small homogeneity range in the binary system Ni-Ti but large Fe solubility by Ni substitution. It is modeled using two sublattices, based on the ideal stoichiometry of the phase.

The Ni₃Ti phase has the D0₂₄ structure (Fig. 1) and shows a remarkable Fe solubility. Its crystal structure might be considered an ordered form of the dhcp A3' structure, which is not stable in Fe-Ni-Ti neither in Al-Fe-Ni-Ti. Therefore it was not possible to model this phase with relation to its disordered counterpart. It is then modeled with two sublattices with site ratio 1/3 where all the three elements can substitute each other in order to reproduce the experimental solubility range.

4. Binary systems

4.1. Fe-Ni

The Fe-Ni phase diagram as assessed by Cacciamani et al. [1] is shown in Fig. 2. The main features are the A1 γ -(Fe, Ni) solid solution which extends, at high temperature, in the whole composition range and the structural and magnetic ordering transformations occurring at lower temperature. Phase relations at temperatures lower than about 300 °C have been mainly studied by investigating meteoric samples, but they are poorly known because at these temperatures thermodynamic equilibrium can hardly be achieved even at geological time scales. In particular

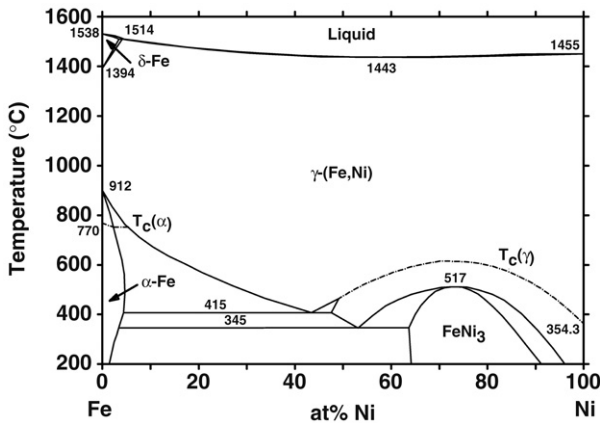


Fig. 2. The critically assessed Fe–Ni phase diagram [1].

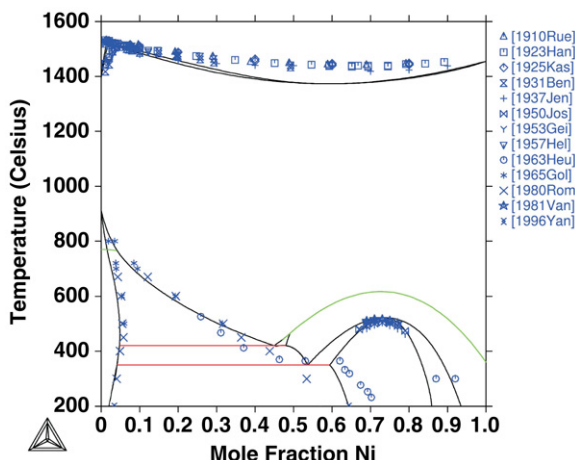


Fig. 3. Stable phase diagram of Fe–Ni according to Cacciamani and Dinsdale [16] compared to experiments by Ruerand and Schuz [1910Rue, [17]], Hanson and Freeman [1923Han, [18]], Kase [1925Kas, [19]], Bennedek and Schafmeister [1931Ben, [20]], Jenkins et al. [1937Jen, [21]], Joso [1950Jos, [22]], Geisler [1959Gei, [23]], Hellawel and Hume-Rothery [1957Hel, [24]], Heumann and Karsten [1963Heu, [25]], Goldstein and Ogilvie [1965Gol, [26]], Romig and Goldstein [1980Rom, [27]], Van Deen and Van der Woude [1981Dee, [28]] and Yang et al. [1996Yan, [13]].

it is still not clear whether the L₁₀ FeNi phase is stable or metastable. According to experimental studies by Yang et al. [13], it is a metastable phase while according to recent ab-initio calculations [14,15] it is weakly stable, but with a driving force in the order of the uncertainty of the calculations. In this study, in agreement with [13], it has been assumed that it is metastable at least for $T > 200$ °C.

A new thermodynamic optimization of the Fe–Ni system is in progress, within the COST 535 action, by Cacciamani and Dinsdale [16], who included a four-sublattice description of the stable (L₁₂ FeNi₃) and metastable (L₁₀ FeNi and L₁₂ Fe₃Ni) ordered phases related to the disordered γ-phase. Preliminary results have been used here.

The stable phase diagram calculated according to the preliminary results by Cacciamani and Dinsdale [16] is shown in Fig. 3. Even if more work is needed to improve the computed Fe–Ni phase diagram (see for inst. the discrepancy between computed and experimental melting equilibria), Fe–Ni phase models and Gibbs energy functions from [16] have been considered more appropriate and reliable than those previously available in literature.

The calculated enthalpy of mixing for the liquid and the solid phases is shown in Fig. 4 for the liquid and in Fig. 5 for the fcc phase.

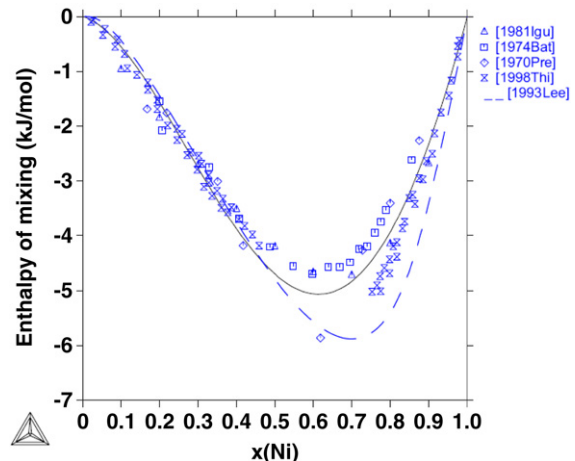


Fig. 4. Enthalpy of mixing for liquid Fe–Ni alloys calculated by Cacciamani and Dinsdale [16] (continuous line) and Lee [1993Lee, [33]] (dashed line) compared to data points from Predel and Mohs [1970Pre, [29]], Batalin et al. [1974Bat, [30]], Iguchi et al. [1981Igu, [31]] and Thiedemann et al. [1998Thi, [32]].

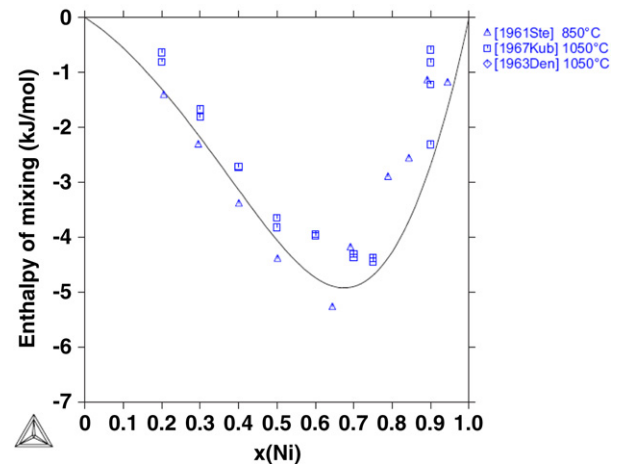


Fig. 5. Enthalpy of mixing for the fcc phase in Fe–Ni alloys calculated according to Cacciamani and Dinsdale [16] (continuous line) compared with experimental data from Steiner and Krisment [1961Ste, [34]], Kubaschewski and Stuart [1967Kub, [35]] and Dench [1963Den, [36]].

4.2. Fe–Ti

The Fe–Ti phase diagram resulting from the critical assessment of Cacciamani et al. [1] is shown in Fig. 6. The most recent thermodynamic assessments were achieved by Kumar et al. [37] and Balun [38]. Kumar et al. used a 2 sublattice model for the B2 FeTi phase, thus allowing for the description of its homogeneity range which was not described in the previous works. The Gibbs energy of this phase was coupled with the Gibbs energy of the disordered bcc phase (A2) that is stable on both the Ti- and Fe-rich sides. This way the order-disorder transformation between the bcc phases can be described. Also the magnetic contribution to the Gibbs energy of the A2 phase was included. Balun [38] has recently performed a similar optimization, which appears in slightly lower agreement with experimental data. The assessment by Kumar et al. [37] is therefore preferred as a starting point. Two improvements, however, appear necessary. One is the 3-sublattice modeling of the C14 Laves phase, the other is the sign of the mixing enthalpy in the hcp phase.

When three sublattices are used for C14 new end-members appear and new parameters need to be evaluated. The Gibbs energy of the stoichiometric stable compound Fe₂Ti remains unchanged:

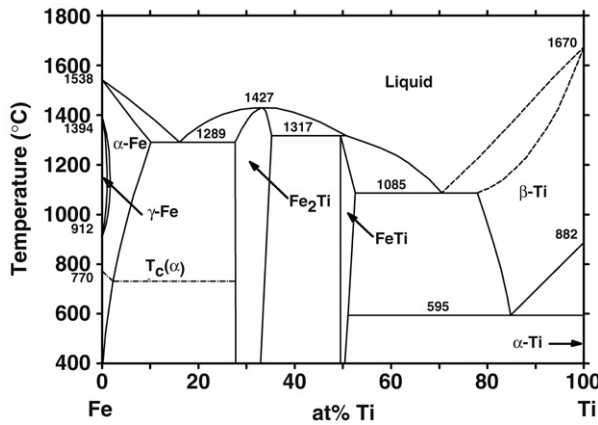


Fig. 6. The critically assessed Fe-Ti phase diagram according to Murray [39].

The Gibbs energy of the other end members is estimated based on simple mechanical mixing of the elements:

$$\begin{aligned} G_{\text{Ti:Fe,Ti}}^{\text{Laves}} &= 1.5G_{\text{Ti}}^{\text{Laves}} + 1.5G_{\text{Fe}}^{\text{Laves}} \\ G_{\text{Fe:Fe,Ti}}^{\text{Laves}} &= 0.5G_{\text{Ti}}^{\text{Laves}} + 2.5G_{\text{Fe}}^{\text{Laves}} \\ G_{\text{Ti:Ti,Fe}}^{\text{Laves}} &= 2.5G_{\text{Ti}}^{\text{Laves}} + 0.5G_{\text{Fe}}^{\text{Laves}} \\ G_{\text{Fe:Ti:Fe}}^{\text{Laves}} &= 1.5G_{\text{Ti}}^{\text{Laves}} + 1.5G_{\text{Fe}}^{\text{Laves}}. \end{aligned} \quad (14)$$

The Gibbs energy for the FeTi₂ compound, as in the original description, was imposed to fulfill the Wagner-Schottky defect model [40], which describes the variation of the Gibbs energy of formation of a compound within a small composition range as a linear function of the amount of the various types of defects. For the Laves phase, modeled with the compound energy formalism, this leads to:

$$G_{\text{Fe:Ti,Ti}}^{\text{Laves}} = 3G_{\text{Ti}}^{\text{Laves}} + 3G_{\text{Fe}}^{\text{Laves}} - G_{\text{TiFe}_2}. \quad (15)$$

As for the mixing parameters, it can be observed that the first sublattice remains unchanged and the interaction parameter derived by Hari Kumar [37] can be kept, while the interaction parameters for the second and third sublattices, resulting from splitting of the former second sublattice, have to be re-evaluated. On the other hand there is no reason to assume a difference in occupation between the second and the third sublattice in C14 Fe₂Ti and it can be assumed that the mixing parameters are equal, taking into account the different number of sites in these sublattices. Then the following equations must hold:

$$\begin{aligned} L_{\text{Fe,Ti:Fe,Ti}}^{\text{Laves}} &= L_{\text{Fe,Ti:Fe,Ti}}^{\text{Laves}} = L_{\text{Fe,Ti,Ti:Fe}}^{\text{Laves}} = L_{\text{Fe,Ti,Ti,Ti}}^{\text{Laves}} \\ L_{\text{Fe:Fe,Ti:Fe,Ti}}^{\text{Laves}} &= L_{\text{Fe:Fe,Ti:Fe,Ti}}^{\text{Laves}} = L_{\text{Ti:Fe,Ti:Fe}}^{\text{Laves}} = L_{\text{Ti:Fe,Ti,Ti}}^{\text{Laves}} \\ L_{\text{Fe:Fe,Fe,Ti}}^{\text{Laves}} &= L_{\text{Fe:Fe,Ti:Fe,Ti}}^{\text{Laves}} = L_{\text{Ti:Fe,Fe,Ti}}^{\text{Laves}} = L_{\text{Ti,Ti:Fe,Ti}}^{\text{Laves}} \end{aligned} \quad (16)$$

The second remark on the description from Kumar et al. [37] is the difference in sign between the interaction parameters at low temperature for fcc A1 and hcp A3 phases. Since both of them are close packed structures with similar coordination, similar interactions between the elements are expected. No thermodynamic data are available for the hcp phase and it is only stable in a small temperature and composition range close to pure Ti, which makes its Fe-Ti interaction parameter poorly determined. Therefore the hcp interaction parameter has been modified by imposing the same sign as the corresponding fcc parameter at low temperature keeping the value of the total hcp Gibbs energy at 900 K about equal to the value obtained by [37]. This change did not appreciably affect the stable equilibria.

The Fe-Ti phase diagram calculated with the new description for the Laves phase and the modified hcp interaction parameter is

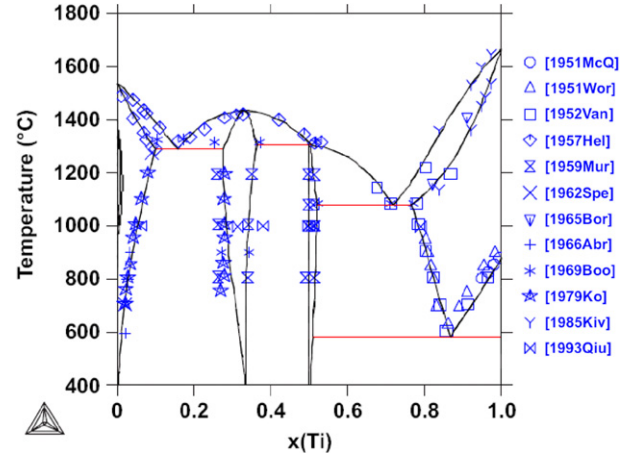


Fig. 7. The Fe-Ti phase diagram calculated in this work. After changes to the underlying models almost coincides with the previous optimisation by Kumar et al. [37]. Experimental data are from McQuillan [1951McQ, [41]], Worner [1951Wor, [42]], Van Thyne et al. [1952Thy, [43]], Hellawell and Hume-Rothery [1957Hel, [24]], Murakami et al. [1959Mur, [44]], Speich [1962Spe, [45]], Boriskina and Kornilov [1965Bor, [46]], Abrahamson and Lopata [1966Abr, [47]], Booker [1969Boo, [48]], Ko and Nishizawa [1979Ko, [49]], Kivilahti and Tarasova [1985Kiv, [50]] and Qiu and Jin [1993Qiu, [51]].

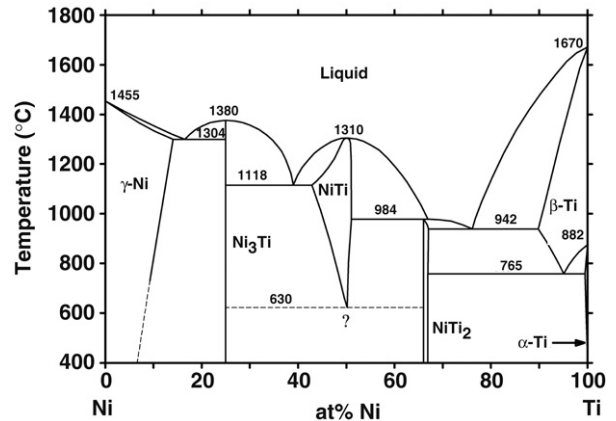


Fig. 8. The critically assessed Ni-Ti phase diagram according to Murray [52].

shown in Fig. 7. It can be noticed that it almost coincides with the phase diagram calculated by Kumar et al. [37]. The present changes, which are important for correct extrapolations, are only visible when looking at the models and the Gibbs energy expressions.

4.3. Ni-Ti

The stable phase diagram as critically assessed by Murray [52] is shown in Fig. 8. Bcc Ti and the fcc Ni solid solutions show up to 10% solubility for the other element while hcp Ti has a very low solubility for Ni. Three intermetallic compounds are formed: Ni₃Ti, NiTi and NiTi₂. Ni₃Ti and NiTi are melting congruently while NiTi₂ is formed peritectically. At low temperatures (<80 °C) and equiatomic composition a martensitic phase with a B19' structure is formed. The presence of this phase gives rise to the well-known shape-memory effect of Ni-Ti alloys.

Murray [52] also assessed thermochemical data for this system, which include Gibbs energies of formation for the different compounds and enthalpy of mixing for the liquid phase. More recently, two new investigations of the enthalpy of mixing were performed by Lück et al. [53] and Thiedeman et al. [54]. The results of their measurements, together with previous measurements from Esin et al. [55], are shown in Fig. 9.

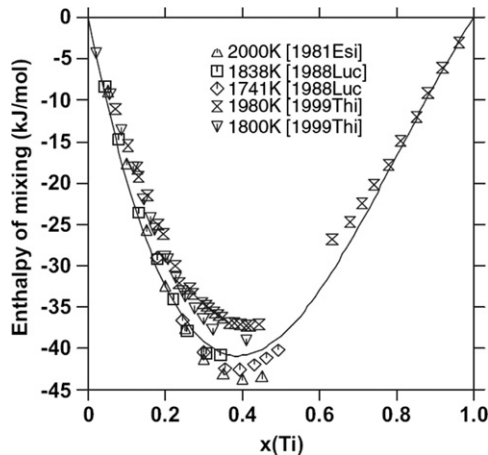


Fig. 9. Enthalpy of mixing for liquid Ni-Ti alloys calculated according to Bellen et al. [56] (continuous line) compared with experimental data from Esin et al. [1981Esi, [55]], Lück [1988Lück, [53]] et al. and Thiedeman et al. [1999Thi, [54]].

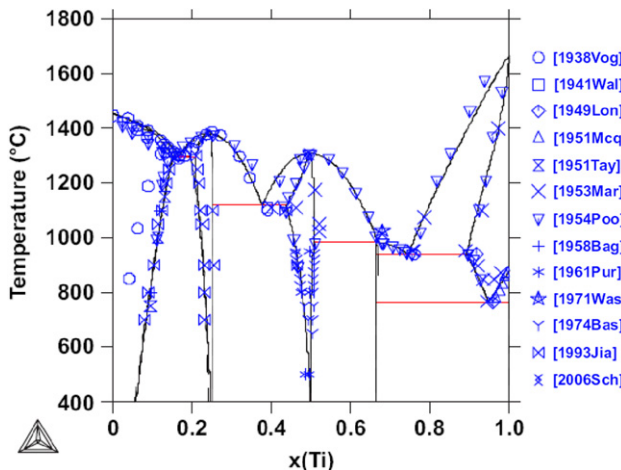


Fig. 10. The Ni-Ti phase diagram calculated in this work. After changes to the underlying models, almost coincides with the previous optimization by Bellen et al. [56]. Experimental data by Vogel and Wallbaum [1938Vog, [2]], Wallbaum and Vogel, [1941Wal, [58]], Long et al. [1949Lon, [59]], McQuillan [1951McQ, [41]], Taylor and Floyd [1951Tay, [60]], Margolin et al. [1953Mar, [61]], Poole and Hume-Rothery [1954Poo, [62]], Bagariatskii and Tiapkin [1957Bag, [63]], Purdy and Gordon [1961Pur, [64]], Wasilewski et al. [1971Was, [65]], Bastin and Rieck [1974Bas, [66]], Jia et al. [1993Jia, [67]] and Schüster [2006Sch, [68]].

The most recent thermodynamic assessments for this system were performed by Bellen et al. [56] and Tang et al. [57]. Both authors describe the B2 phase as an ordered form of the A2 phase. Tang et al. [57] also included the B19' phase, but the optimization from Bellen et al. [56] shows better agreement with experiments. The calculated phase diagram according to Bellen et al. [56] is shown in Fig. 10 while the enthalpy of mixing according to this optimization is shown in Fig. 9. The optimization from Bellen [56] has been chosen as a starting point for further improvements while magnetic parameters for the bcc phases have been taken from Tang et al. [57]. Since the Laves phase and the ordered fcc phases are metastable in this system, they were not included in the description by Bellen [56]. These parameters were subsequently introduced by Ansara et al. [69] and are taken from there.

During the present investigation it was noticed that the Ni₃Ti phase becomes stable at higher temperatures close to pure Ni when the phase diagram is calculated from the description by Bellen. The lattice stabilities used for the pure elements in the description of this phase were thought to be the main reason to this problem; they were thus changed. In Bellen's description, the

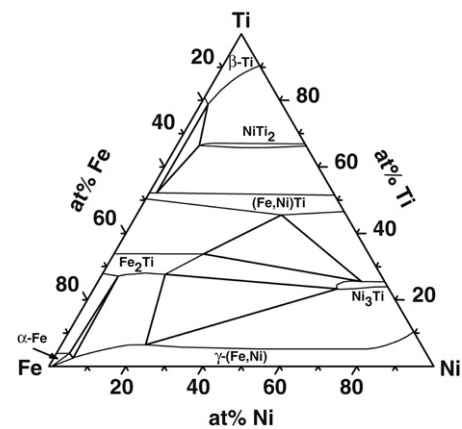


Fig. 11. Fe-Ni-Ti isothermal section at 900 °C experimentally determined by Van Loo et al. [71].

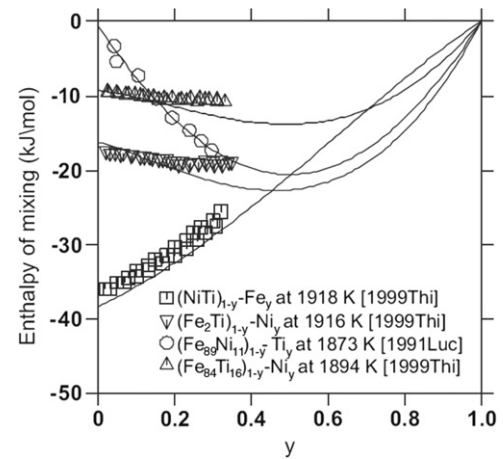


Fig. 12. Enthalpy of mixing for the Fe-Ni-Ti liquid phase calculated in this work compared to experimental data points from Thiedemann et al. [1999Thi, [54]] and Lück et al. [1991Lück, [75]].

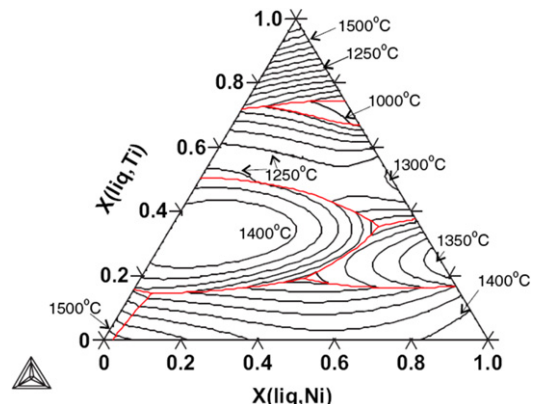


Fig. 13. Fe-Ni-Ti liquidus projection calculated in this work.

Ni₃Ti compound was modeled using, for the pure elements, the Gibbs energy expression used for the hcp phase. However, it can be noticed (see Fig. 1) that in the Ni₃Ti structure half of the atoms have the anti-cuboctahedral coordination typical of hcp, while the other half has the cuboctahedral coordination typical of the fcc structure. Actually, when all the atomic positions in the Ni₃Ti structure are occupied by the same element the A3' dhcp structure is obtained. Therefore the Gibbs energy expression for the pure elements in the Ni₃Ti structure should refer to the dhcp instead of the hcp phase.

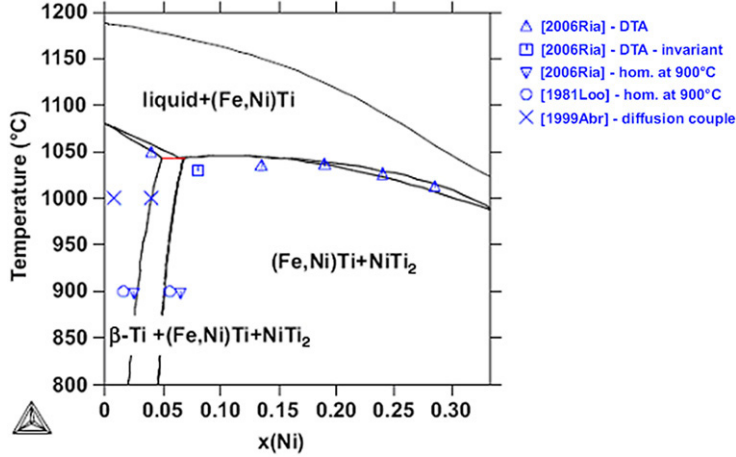


Fig. 14. Vertical section at 66 at.% Ti calculated in this work compared to experimental data from Riani et al. [2006Ria, [74]], Van Loo et al. [1981Loo, [71]] and Abramaycheva et al. [1999Abr, [73]].

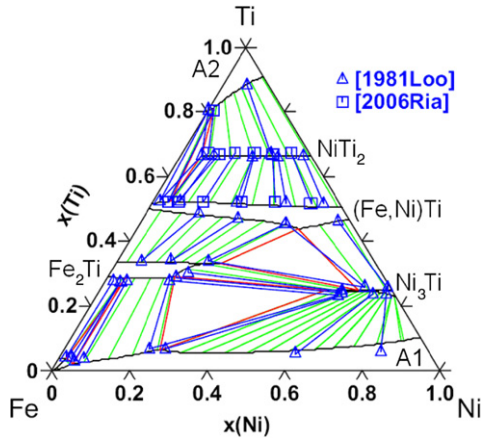


Fig. 15. Fe–Ni–Ti isothermal section at 900 °C calculated in this work compared to experimental tie lines and tie triangles from Van Loo et al. [1981Loo, [71]] and Riani et al. [2006Ria, [74]].

Since no value for the lattice stability of dhcp Ni and Ti is available, it was assumed:

$$G_i^{dhcp} = \frac{1}{2} G_i^{fcc} + \frac{1}{2} G_i^{hcp}. \quad (17)$$

This expression cannot be understood as a general rule as in some cases (La for instance) the dhcp phase is more stable than the other two. Nevertheless, it is thought it could be a reasonable estimation if no other reliable value is available.

After changing the Gibbs energy of the pure element end members, parameters for Ni₃Ti were re-assessed using a limited set of experimental data, namely values for the congruent melting of Ni₃Ti, the solubility range of this phase and the invariant reactions involving Ni₃Ti. As a consequence the parameters for the disordered fcc (A1) phase were also re-evaluated because their values influence the relative stability of the Ni₃Ti phase on the Ni-rich side.

As far as the NiTi₂ phase is concerned, the Gibbs energy of formation of the antistructural compound and the lattice stabilities of the pure elements in the NiTi₂ structure have been assumed equal to the corresponding values used for the Laves phase.

Fig. 10 shows the calculated phase diagram: just as for the Fe-Ti system, the changes mentioned above do not appreciably affect the stable phase equilibria, but are only visible when looking at the models and Gibbs energy expressions.

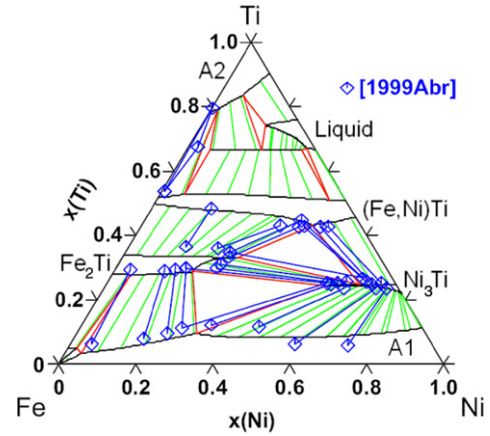


Fig. 16. Fe–Ni–Ti isothermal section at 1000 °C calculated in this work compared with experimental tie lines and tie triangles from Abramaycheva et al. [1999Abr, [73]].

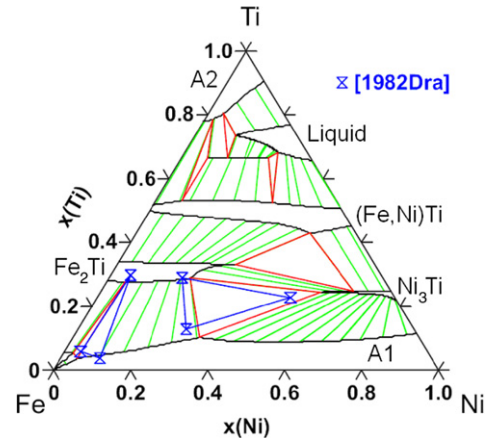


Fig. 17. Fe–Ni–Ti isothermal section at 1300 °C calculated in this work compared with experimental tie triangles from Drake et al. [1982Dra, [76]].

5. Ternary system

The Fe–Ni–Ti system was recently critically assessed by Cacciamani et al. [1]. Key investigations of the Fe–Ni–Ti phase equilibria have been done by Vogel and Wallbaum [2], Dudkina and Kornilov [70], Van Loo et al. [71], Alisova et al. [72], Abramaycheva et al. [73], Riani et al. [74] for phase diagram data and by Thiedeman

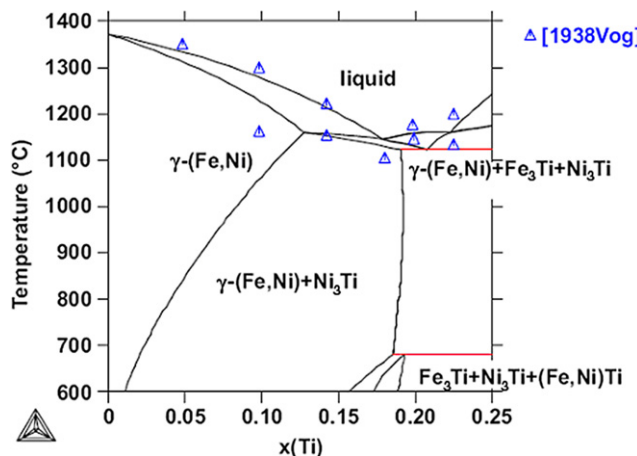


Fig. 18. Partial Fe–Ni–Ti vertical section at $w(\text{Fe})/w(\text{Ni}) = 4/6$ calculated in this work compared with experimental data points from Vogel and Walbaum [1938Vog, 2].

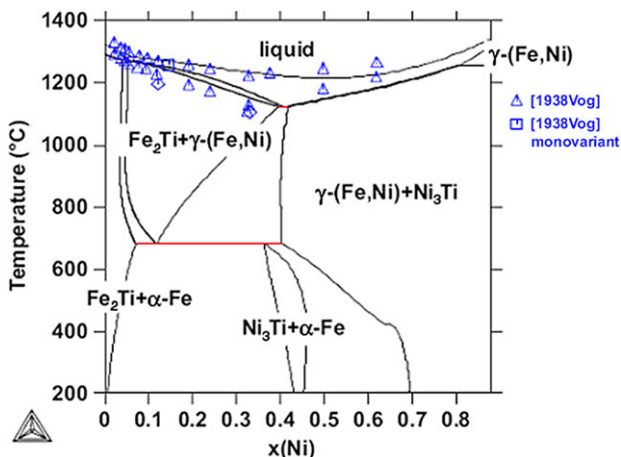


Fig. 19. Fe–Ni–Ti vertical section at 12 wt% Ti calculated in this work compared with experimental data points from Vogel and Walbaum [2].

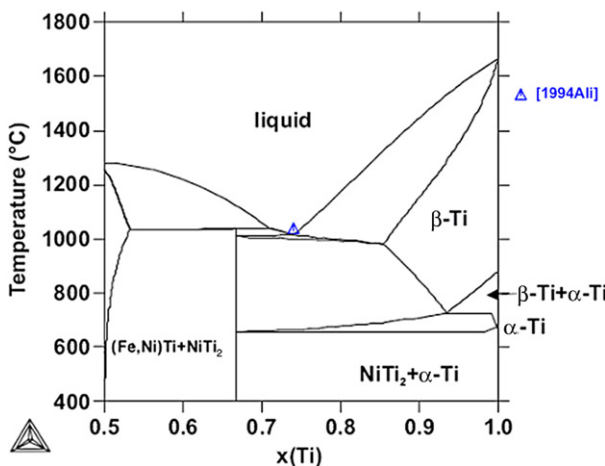


Fig. 20. Partial Fe–Ni–Ti vertical section at $x(\text{Fe})/x(\text{Ni}) = 1$ calculated in this work compared with one data point read from the vertical section by Alisova et al. [72].

et al. [54] for enthalpy measurements. No ternary phase is present in the Fe–Ni–Ti system while binary Ni_3Ti , NiTi_2 and Fe_2Ti phases show large solubility of the third element and form homogeneous fields extending in the ternary at almost constant Ti content. Structural data of the binary phases and their extension in the ternary system are summarized in Table 1.

NiTi_2 dissolves so much Fe that its solubility range extends very close to the Fe–Ti binary, as shown in the experimental 900 °C

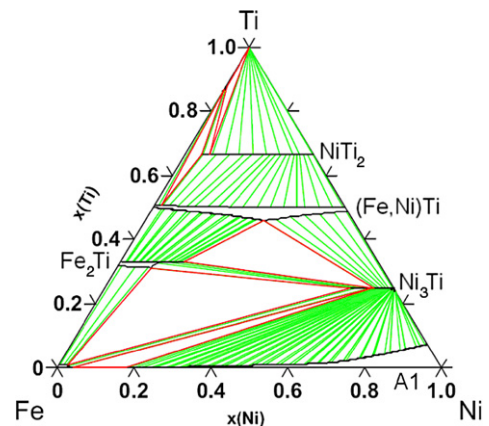


Fig. 21. Fe–Ni–Ti isothermal section at 600 °C calculated in this work.

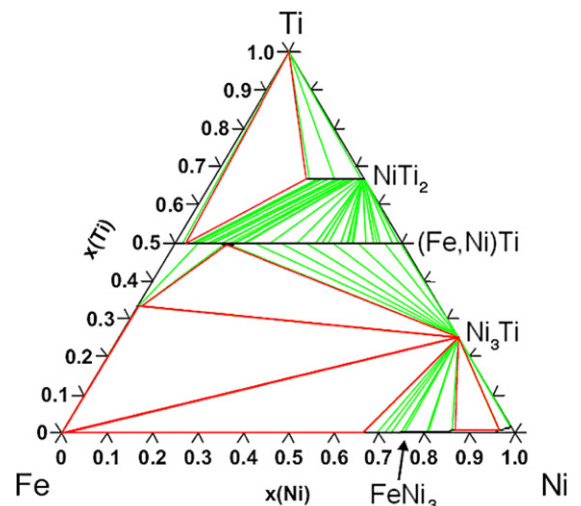


Fig. 22. Fe–Ni–Ti isothermal section at 100 °C calculated in this work.

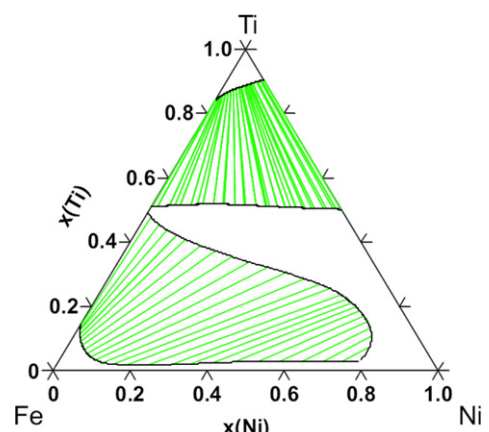


Fig. 23. Metastable Fe–Ni–Ti isothermal equilibria between ordered and disordered bcc phases calculated in this work at 700 °C.

isothermal section presented in Fig. 11. It is however incomplete, no FeTi_2 compound being stable in the Fe–Ti system.

NiTi and FeTi are isostructural (B2 structure) and form a continuous solid solution crossing the phase diagram at about 50 at.% Ti. Close to the Fe–Ni binary subsystem the $\gamma-(\text{Fe}, \text{Ni})$ solid solution dissolves a few at.% of Ti.

Table A.1

Gibbs energy expressions for the elements.

Function	Value	Temp. range and reference ^a
GHSERFE	$+1225.7 + 124.134*T - 23.5143*T*LN(T) - .00439752*T**2 - 5.8927E - 08*T**3 + 77359*T**(-1);$ $-25383.581 + 299.31255*T - 46*T*LN(T) + 2.29603E + 31*T**(-9);$	$T > 298\text{ K}$ $T > 1811\text{ K}$
GHSERNI	$-5179.159 + 117.854*T - 22.096*T*LN(T) - .0048407*T**2;$ $-27840.655 + 279.135*T - 3.1*T*LN(T) + 1.12754E + 31*T**(-9);$	$T > 298\text{ K}$ $T > 1728\text{ K}$
GHSERTI	$-8059.921 + 133.615208*T - 23.9933*T*LN(T) - .004777975*T**2 + 1.06716E - 07*T**3 + 72636*T**(-1);$ $-7811.815 + 132.988068*T - 23.9887*T*LN(T) - .0042033*T**2 - 9.0876E - 08*T**3 + 42680*T**(-1);$ $+908.837 + 66.976538*T - 14.9466*T*LN(T) - .0081465*T**2 + 2.02715E - 07*T**3 - 1477660*T**(-1);$ $-124526.786 + 638.806871*T - 87.2182461*T*LN(T) + .008204849*T**2 - 3.04747E - 07*T**3 + 36699805*T**(-1);$	$T > 298\text{ K}$ $T > 900\text{ K}$ $T > 1155\text{ K}$ $T > 1941\text{ K}$
GBCCFE	$+GHSERFE;$	
GBCCNI	$+8715.084 - 3.556*T + GHSERNI;$	
GBCCTI	$-1272.064 + 134.71418*T - 25.5768*T*LN(T) - 6.63845E - 04*T**2 - 2.78803E - 07*T**3 + 7208*T**(-1);$ $+6667.385 + 105.366379*T - 22.3771*T*LN(T) + .00121707*T**2 - 8.4534E - 07*T**3 - 2002750*T**(-1);$ $+26483.26 - 182.426471*T + 19.0900905*T*LN(T) - .02200832*T**2 + 1.228863E - 06*T**3 + 1400501*T**(-1);$	$T > 298\text{ K}$ $T > 1155\text{ K}$ $T > 1941\text{ K}$
GFCCFE	$-236.7 + 132.416*T - 24.6643*T*LN(T) - .00375752*T**2 - 5.8927E - 08*T**3 + 77359*T**(-1);$ $-27097.3963 + 300.252559*T - 46*T*LN(T) + 2.78854E + 31*T**(-9);$	$T > 298\text{ K}$ $T > 1811\text{ K}$
GFCCNI	$+GHSERNI;$	
GFCTTI	$+6000 - .1*T + GHSERTI;$	
GHCPFE	$-2480.08 + 136.725*T - 24.6643*T*LN(T) - .00375752*T**2 - 5.8927E - 08*T**3 + 77359*T**(-1);$ $-29340.776 + 304.561559*T - 46*T*LN(T) + 2.78854E + 31*T**(-9);$	$T > 298\text{ K}$ $T > 1811\text{ K}$
GHCPTI	$+GHSERTI;$	
DGLAV	5000;	
GLAVFE	$+GHSERFE + DGLAV;$	
GLAVNI	$+GHSERNI + DGLAV;$	
GLAVTI	$+GHSERTI + DGLAV;$	
GDHCFE	$.5*GHCPFE + .5*GFCCFE;$	This work
GDHCNI	$.5*GHCPTI + .5*GFCCNI;$	This work
GDHCTI	$.5*GHCPTI + .5*GFCTTI;$	This work

^a Default temperature range is 298 K < T < 3000 K. Default reference is [77].

6. Assessment procedure

As a first step in the assessment of the ternary system a database was constructed based on the binary sub-systems. Experimental data to be used for the optimization were selected based on the critical assessment of Cacciamani et al. [1]. From the vertical sections of Vogel and Wallbaum [2], only the data involving liquid were used. The 900 °C isothermal section from Van Loo et al. [71] was used completely. Also all data along the section at 66 at.% Ti from Riani et al. [74] were included. From Abramhycheva [73], only the tie-triangles were used. The points on the solidus line in the section NiTi–FeTi from Dudkina [70] were used but the possibility of large errors was kept in mind and a lower weight was given to these data. Enthalpies of mixing in liquid measured by Lück et al. [75] and Thiedeman et al. [54] were also used.

After the treatment of the different regions separately, a minimization run including all parameters was performed in order to obtain a global minimization. Parameters were then rounded to a reasonable number of significant digits.

6.1. Liquid

Experimentally determined enthalpies of mixing [75,54] together with liquidus points from Vogel [2] were used to evaluate

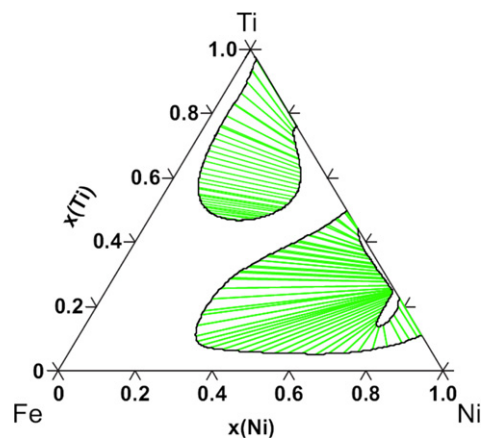


Fig. 24. Metastable Fe–Ni–Ti isothermal equilibria between ordered and disordered fcc phases calculated in this work at 700 °C.

the temperature-independent part of the ternary interaction parameter for the liquid phase. A temperature-dependent variable did not bring significant amelioration to the description and was therefore omitted.

Table A.2

Gibbs energy expressions for the Fe–Ni system.

Parameter	Value	Reference
G(LIQUID, FE, NI;0)	$-18782 + 3.7011 \cdot T$	[16]
G(LIQUID, FE, NI;1)	$+12308.6 - 2.75998 \cdot T$	[16]
G(LIQUID, FE, NI;2)	$+4457 - 4.1536 \cdot T$	[16]
G(A1, FE, NI:VA;0)	$-14084 + 3.27413 \cdot T$	[16]
G(A1, FE, NI:VA;1)	$+14000 - 4.45077 \cdot T$	[16]
G(A1, FE, NI:VA;2)	-3000	[16]
TC(A1, FE, NI:VA;0)	$+2133$	[16]
TC(A1, FE, NI:VA;1)	-682	[16]
BMAGN(A1, FE, NI:VA;0)	9.55	[16]
BMAGN(A1, FE, NI:VA;1)	7.25	[16]
BMAGN(A1, FE, NI:VA;2)	5.93	[16]
BMAGN(A1, FE, NI:VA;3)	6.18	[16]
G(FCC4, FE2NI2) ^a	$6500 + 2.5 \cdot T$	[16]
G(FCC4, FENI3) ^a	$-9470 + 3.1 \cdot T$	[16]
G(FCC4, FE3NI) ^a	0	[16]
TC(FCC4, FE2NI2) ^a	245	[16]
TC(FCC4, FENI3) ^a	245	[16]
TC(FCC4, FE3NI) ^a	0	[16]
BMAG(FCC4, FE2NI2) ^a	0.115	[16]
BMAG(FCC4, FENI3) ^a	0.115	[16]
BMAG(FCC4, FE3NI) ^a	0	[16]
G(A2, FE, NI:VA;0)	$-956.63 - 1.28726 \cdot T$	[16]
G(A2, FE, NI:VA;1)	$+3789.03 - 1.92912 \cdot T$	[16]
TC(A2, FE, NI:VA;0)	-1000	[16]
TC(A2, FE, NI:VA;1)	1500	[16]
BMAGN(A2, FE, NI:VA;0)	1	[16]
BMAGN(A2, FE, NI:VA;1)	1.6	[16]
G(BCC2, FENI) ^b	0	This work
G(A3, FE, NI:VA;0)	$-12054.355 + 3.27413 \cdot T$	[16]
G(A3, FE, NI:VA;1)	$+11082 - 4.45077 \cdot T$	[16]
G(A3, FE, NI:VA;2)	-725.8	[16]
G(C14, NI:FE:FE;0)	$-15000 + GLAVNI + 2 \cdot GLAVFE$	This work
G(C14, FE:NI:FE;0)	$+1.5 \cdot GLAVFE + 1.5 \cdot GLAVNI$	This work
G(C14, NI:NI:FE;0)	$+0.5 \cdot GLAVFE + 2.5 \cdot GLAVNI$	This work
G(C14, FE:FE:NI;0)	$+2.5 \cdot GLAVFE + .5 \cdot GLAVNI$	This work
G(C14, NI:FE:NI;0)	$+1.5 \cdot GLAVFE + 1.5 \cdot GLAVNI$	This work
G(C14, FE:NI:NI;0)	$-29828 + GLAVFE + 2 \cdot GLAVNI$	This work
G(C15, NI:FE;0)	$+GLAVNI + 2 \cdot GLAVFE$	[16]
G(C15, FE:NI;0)	$+GLAVFE + 2 \cdot GLAVNI$	[16]
G(C36, NI:FE;0)	$+GLAVNI + 2 \cdot GLAVFE$	[16]
G(C36, FE:NI;0)	$+GLAVFE + 2 \cdot GLAVNI$	[16]
G(NI3Ti, NI:FE;0)	$+3 \cdot GDHCNI + GDHCFE$	[16]
G(NI3Ti, FE:NI;0)	$+3 \cdot GDHCFE + GDHCNI$	[16]
G(NiT12, NI:FE;0)	$+GHSERNI + 2 \cdot GHSERFE + 3 \cdot DGLAV$	[16]
G(NiT12, FE:NI;0)	$+2 \cdot GHSERNI + 2 \cdot GHSERNI + 3 \cdot DGLAV$	[16]

^a This parameter denotes all the different distribution of Fe and Ni on the sublattices with the given global composition (see Eq. (10)).

^b This parameter denotes all the different distributions of Fe and Ni on the sublattices with the given global composition (see Eq. (12)).

Calculated and experimental values of the enthalpy of mixing are plotted in Fig. 12 for the sections NiTi–Fe, Fe₂Ti–Ni, Fe₈₉Ni₁₁–Ti and Fe₈₄Ni₁₆–Ti. A general good agreement can be observed. The disagreement of the section NiTi_y–Fe_{1–y} originates from the disagreement between the experimental data used for the optimization of the ternary system [54] and the data used by Bellen [53,55] for the optimization of the binary Ni–Ti system. In fact the data from Thiedemann [54] about both Ni–Ti and Fe–Ni–Ti (not available at the time of the Ni–Ti optimization) are less negative than those by Luck et al. and Esin et al. [53,55] used for the Ni–Ti optimization. This explains the systematic deviation observed in the figure.

Fig. 13 shows the calculated liquidus projection, where monovariant liquidus curves agree with those predicted in the critical review [1].

6.2. Ti-rich region

The Ti-rich region shows the stable equilibria between B2 (ordered bcc), A2 (disordered bcc) and NiTi₂. In order to reproduce

the large Fe solubility range in NiTi₂ not only a negative value was given to the Gibbs energy of the metastable FeTi₂ end member but it was also necessary to add a negative interaction parameter $L_{Ti:Ni,Fe}^{NiTi_2}$ relative to the mixing between Fe and Ni on the second NiTi₂ sublattice, while Ti is on the first one.

As it was already mentioned in the critical assessment [1], the tie-triangle from Abramyczeva [73] was found to be unlikely (Fig. 14) in comparison with the other experiments. Therefore these data were not taken into account for the optimization.

The bcc phase in this region is only characterized in the three phase equilibrium and one tie-line measured by Van Loo [71]. It was possible to reproduce these results without a ternary parameter for this phase.

6.3. Medium Ti region

At 50 at.% Ti, the B2 (Ni, Fe)Ti phase is formed. Data in this region are tie-lines from Van Loo [71] and Abramyczeva [73] (Figs. 15 and 16), and solidus points by Dudkina [70]. An interaction parameter $L(bcc, Fe, Ni:Ti;0)$ was introduced to obtain the right composition

Table A.3

Gibbs energy expressions for the Fe–Ti system.

Parameter	Value	Reference
G(LIQUID, FE, TI;0)	$-76247 + 17.845 \cdot T$	[37]
G(LIQUID, FE, TI;1)	$+7990 - 6.059 \cdot T$	[37]
G(LIQUID, FE, TI;2)	$+4345 - 2.844 \cdot T$	[37]
G(A1, FE, TI:VA;0)	$-56022 + 8.356 \cdot T$	[37]
G(A1, FE, TI:VA;1)	$+4773 - 4.029 \cdot T$	[37]
G(A1, FE, TI:VA;2)	$+30021 - 12.614 \cdot T$	[37]
G(FCC4, TI3FE) ^a	$+3 \cdot \text{UFETI}$	[78]
G(FCC4, TI2FE2) ^a	$+4 \cdot \text{UFETI}$	[78]
G(FCC4, TIFE3) ^a	$+3 \cdot \text{UFETI}$	[78]
UFETI	$-12274 + 8.59 \cdot T$	This work
G(A2, FE, TI:VA;0)	$-68448 + 23.825 \cdot T$	[37]
G(A2, FE, TI:VA;1)	$+5467 - 5.083 \cdot T$	[37]
G(A2, FE, TI:VA;2)	$+25262 - 15.83 \cdot T$	[37]
TC(A2, FE, TI:VA;0)	637.79	[37]
G(BCC2, FETI) ^a	$76218 - 46.685 \cdot T + 8.663 \cdot T \cdot \ln(T) - 0.007151 \cdot T^2 + 1.121169 \cdot 10^{-6} \cdot T^3$	[37]
TC(BCC2, FETI) ^a	-1325	[37]
G(BCC2, FE, TI:FE:VA;0)	-10971	[37]
G(BCC2, FE:FE, TI:VA;0)	-10971	[37]
G(BCC2, FE, TI:FE:VA;1)	-13764	[37]
G(BCC2, FE:FE, TI:VA;1)	-13764	[37]
G(BCC2, TI:FE, TI:VA;0)	-6097	[37]
G(BCC2, FE, TI:TI:VA;0)	-6097	[37]
G(BCC2, TI:FE, TI:VA;1)	12256	[37]
G(BCC2, FE, TI:TI:VA;1)	12256	[37]
G(A3, FE, TI:VA;0)	-10000 + 15 · T	This work
GTIFE2	$-78603 + 349.9675 \cdot T - 64.502 \cdot T \cdot \ln(T) - .0241491 \cdot T^2 + 3.936825 \cdot 10^{-6} \cdot T^3 + 7620 \cdot T^{-1}$	[37]
G(C14, TI:FE:FE;0)	+GTIFE2	[37]
G(C14, FE:TI:TI;0)	$+3 \cdot \text{GHSERFE} + 3 \cdot \text{GHSERTI} + 6 \cdot \text{DGLAV} - \text{GTIFE2}$	[37]
G(C14, FE:TI:FE;0)	$+1.5 \cdot \text{GLAVTI} + 1.5 \cdot \text{GLAVFE}$	This work
G(C14, TI:TI:FE;0)	$+2.5 \cdot \text{GLAVTI} + 0.5 \cdot \text{GLAVFE}$	This work
G(C14, FE:FE:TI;0)	$+0.5 \cdot \text{GLAVTI} + 2.5 \cdot \text{GLAVFE}$	This work
G(C14, TI:FE:TI;0)	$+1.5 \cdot \text{GLAVTI} + 1.5 \cdot \text{GLAVFE}$	This work
G(C14, FE, TI:FE:FE;0)	3177	[37]
G(C14, FE, TI:TI:TI;0)	3177	[37]
G(C14, FE:FE, TI:FE;0)	18000	This work
G(C14, FE:FE:FE, TI;0)	6000	This work
G(C14, TI:FE, TI:FE;0)	18000	This work
G(C14, TI:FE:FE, TI;0)	6000	This work
G(C14, FE:TI:FE, TI;0)	6000	This work
G(C14, TI:TI:FE, TI;0)	6000	This work
G(C14, FE:FE, TI:TI;0)	18000	This work
G(C14, TI:FE, TI:TI;0)	18000	This work
G(NI3TI, TI:FE;0)	$+3 \cdot \text{GDHTI} + \text{GDHCFE} + 30\,000$	[37]
G(NI3TI, FE:TI;0)	$3 \cdot \text{GHSERFE} + \text{GHSERTI} - 33000 + 2 \cdot T$	This work
G(NITI2, TI:FE;0)	$+2 \cdot \text{GHSERTI} + \text{GHSERFE} + 3 \cdot \text{GFTI2FE}$	[37]
G(NITI2, FE:TI;0)	$+2 \cdot \text{GHSERFE} + \text{GHSERTI} + 6 \cdot \text{DGLAV}$	[37]
GFTI2FE	-17202 + 1.2	This work
G(NITI2, FE, TI:FE;0)	60000	[37]
G(NITI2, FE:FE, TI;0)	60000	[37]
G(NITI2, TI:FE, TI;0)	60000	[37]
G(NITI2, FE, TI:TI;0)	60000	[37]

^a This parameter denotes all the different distribution of Fe and Ti on the sublattices with the given global composition (see Eq. (12)).

for the (Ni, Fe)Ti phase in the three phase equilibria (Ni, Fe)Ti + β -Ti + NiTi₂ and (Ni, Fe)Ti + Ni₃Ti + Fe₂Ti (C14).

6.4. Low Ti region

The introduction of 3 sublattices for the Laves phase required the evaluation of new metastable binary and ternary end members. At first, a standard value (equal to mechanical mixing of the pure elements in the Laves structure) was given for the Gibbs energies of all these compounds. However, few of them have been optimized in order to reproduce the solubility of Ni in Fe₂Ti. In particular it was necessary to evaluate selected Fe–Ni binary parameters and a few ternary parameters. With these parameters, solubility could be described reasonably well.

The solubility of Fe in the Ni₃Ti phase was fitted to the experiments by assessment of the Gibbs energy of formation of the metastable Fe₃Ti end member.

Since there are no ternary data on the solubility of Ti in the FeNi₃ phase, no optimization was done for this phase.

In this region, the A2 phase is stable in the form of α -Fe. No experimental data in the ternary system are available here and therefore no ternary interaction is introduced.

The disordered fcc (A1) is stable in the form of γ -(Fe, Ni) and mainly determined by experimental tie-lines from Van Loo [71] and Abramyczeva [73] (Figs. 15 and 16). A ternary interaction parameter L(A1, Fe, Ni, Ti:Va;0) was introduced to describe the Ti-solubility in this phase.

6.5. Calculated sections and Scheil diagram

The resulting database is given in the Appendix. From this database different sections can be calculated and compared with experimental results. Figs. 14–20 show the calculated sections together with experimental results. An overall good agreement

Table A.4

Gibbs energy expressions for the Ni–Ti system.

Parameter	Value	Reference
G(LIQUID, NI, TI;0)	$-153707.39 + 34.859449 \cdot T$	[56]
G(LIQUID, NI, TI;1)	$-81824.755 + 25.809901 \cdot T$	[56]
G(LIQUID, NI, TI;2)	$-10.077897 \cdot T$	[56]
G(A1, NI, TI:VA;0)	$-98143 + 6.706 \cdot T$	This work
G(A1, NI, TI:VA;1)	-62430	This work
TC(A1, NI, TI:VA;0)	-2500	This work
TC(A1, NI, TI:VA;1)	-3000	This work
TC(A1, NI, TI:VA;2)	$+1300$	This work
G(FCC4, TiNi3) ^a	$3 \cdot \text{UNITI}$	[79]
G(FCC4, Ti2Ni2) ^a	$4 \cdot \text{UNITI} + 30466$	[79]
G(FCC4, Ti3Ni) ^a	$3 \cdot \text{UNITI}$	[79]
UNITI	$-8562 + 4.1 \cdot T$	[79]
G(FCC4, NI, Ti) ^b	-5408	[79]
G(A2, NI, TI:VA;0)	$-97427 + 12.112 \cdot T$	[56]
G(A2, NI, TI:VA;1)	-32315	[56]
TC(A2, NI, TI:VA;0)	-575	[56]
BMAGN(A2, NI, TI:VA;0)	-0.85	[56]
G(BCC2, NiTi) ^c	$-33193.7 + 10.284 \cdot T$	[56]
G(BCC2, Ti:NI, Ti:VA;0)	$+60723.7 - 15.4024 \cdot T$	[56]
G(BCC2, Ni, Ti:Ti:VA;0)	$+60723.7 - 15.4024 \cdot T$	[56]
G(BCC2, Ni, Ti:Ni:VA;0)	$-55288.8 + 25.4416 \cdot T$	[56]
G(BCC2, Ni:Ni, Ti:VA;0)	$-55288.8 + 25.4416 \cdot T$	[56]
G(BCC2, Ni:Ni, Ti:VA;2)	$+6010.11 + 3.95974 \cdot T$	[56]
G(BCC2, Ni, Ti:Ni:VA;2)	$+6010.11 + 3.95974 \cdot T$	[56]
G(A3, NI, Ti:VA;0)	-20000	[56]
G(C14, Ti:NI:NI;0)	$+GHSERTI + 2 \cdot GHSERNI + 3 \cdot GFTINI2$	This work
G(C14, NI:Ti:Ti;0)	$+GLAVNI + 2 \cdot GLAVTI + 3 \cdot DGLAV - 3 \cdot GFTINI2$	This work
GFTINI2	$-2.7132753E + 04;$	This work
G(C14, Ti:Ti:NI;0)	$+2.5 \cdot GLAVTI + 0.5 \cdot GLAVNI$	This work
G(C14, NI:NI:Ti;0)	$+5 \cdot GLAVTI + 2.5 \cdot GLAVNI$	This work
G(C14, Ti:NI:Ti;0)	$+1.5 \cdot GLAVTI + 1.5 \cdot GLAVNI$	This work
G(NiT12, Ti:NI;0)	$+3 \cdot GTI2NI$	[69]
G(NiT12, Ni:Ti;0)	$+2 \cdot GLAVNI + GLAVTI + 30000 - 3 \cdot GTI2NI$	[69]
GTI2NI	$.333333 \cdot GHSERNI + .666667 \cdot GHSERTI - 27514.218 + 2.85345219 \cdot T$	[69]
G(NiT12, Ni, Ti:NI;0)	60000	[56]
G(NiT12, Ni:Ni, Ti;0)	60000	[56]
G(NiT12, Ti:NI, Ti;0)	60000	[56]
G(NiT12, Ni, Ti:Ti;0)	60000	[56]
G(Ni3Ti, Ni:Ti;0)	$4 \cdot (-39436 + 4.6636 \cdot T) + 3 \cdot GDHCNI + GDHCTI$	This work
G(Ni3Ti, Ti:NI;0)	$-4 \cdot (-39436 + 4.6636 \cdot T) + GDHCNI + 3 \cdot GDHCTI$	This work
G(Ni3Ti, Ni:NI, Ti;0)	$+4 \cdot (+35804 - 25.444 \cdot T)$	This work
G(Ni3Ti, Ni:NI, Ti;1)	$+4 \cdot (+27289 - 16.612 \cdot T)$	This work
G(Ni3Ti, Ti:NI, Ti;0)	$+20000$	[56]
G(Ni3Ti, Ni, Ti:Ti;0)	$+60000$	[56]

^a This parameter denotes all the different distribution of Ni and Ti on the sublattices with the given global composition (see Eq. (10)).^b This parameter denotes all the interaction between Ni and Ti on one sublattice, for each of the sublattices (see Eq. (11)).^c This parameter denotes all the different distribution of Ni and Ti on the sublattices with the given global composition (see Eq. (12)).**Table A.5**

Gibbs energy expressions for the Fe–Ni–Ti system.

Parameter	Value	Reference
G(LIQUID, FE, NI, TI;0)	17749	This work
G(A1, FE, NI, TI:VA;0)	17818	This work
G(BCC2, Ti:FE, NI:VA;0)	11774	This work
G(BCC2, FE, NI:Ti:VA;0)	11774	This work
G(C14, Ti:FE:NI;0)	$-92832 + 2.646 \cdot T + GLAVTI + 1.5 \cdot GLAVFE + 0.5 \cdot GLAVNI$	This work
G(C14, FE:Ti:NI;0)	$+GLAVFE + 1.5 \cdot GLAVTI + 0.5 \cdot GLAVNI$	This work
G(C14, NI:FE:Ti;0)	$+GLAVNI + 1.5 \cdot GLAVFE + 0.5 \cdot GLAVTI$	This work
G(C14, Ti:FE:Ti;0)	$+1.5 \cdot GLAVTI + 1.5 \cdot GLAVFE$	This work
G(C14, FE:NI:Ti;0)	$+GLAVFE + 1.5 \cdot GLAVNI + .5 \cdot GLAVTI$	This work
G(C14, Ti:NI:FE;0)	$-97167 + 7.11 \cdot T + GLAVTI + 1.5 \cdot GLAVNI + 0.5 \cdot GLAVFE$	This work
G(C14, NI:Ti:FE;0)	$+GLAVNI + 1.5 \cdot GLAVTI + 0.5 \cdot GLAVFE$	This work
G(NiT12, Ti:FE, NI;0)	$-7664 + 9.225 \cdot T$	This work

could be obtained and the optimization confirms the assessed sections of the phase diagram from the critical review [1]. From the assessed description, metastable equilibria and sections for which no experimental data are available can now be calculated (Figs. 21–24). The section at 100 °C (Fig. 22) shows the predicted equilibria

with the low temperature L1₂FeNi₃ compound. Figs. 23 and 24 show the metastable equilibria between ordered and disordered phases based on fcc and bcc, respectively. Since for bcc only two sublattices were used, only the ordered phase at equiatomic composition is found.

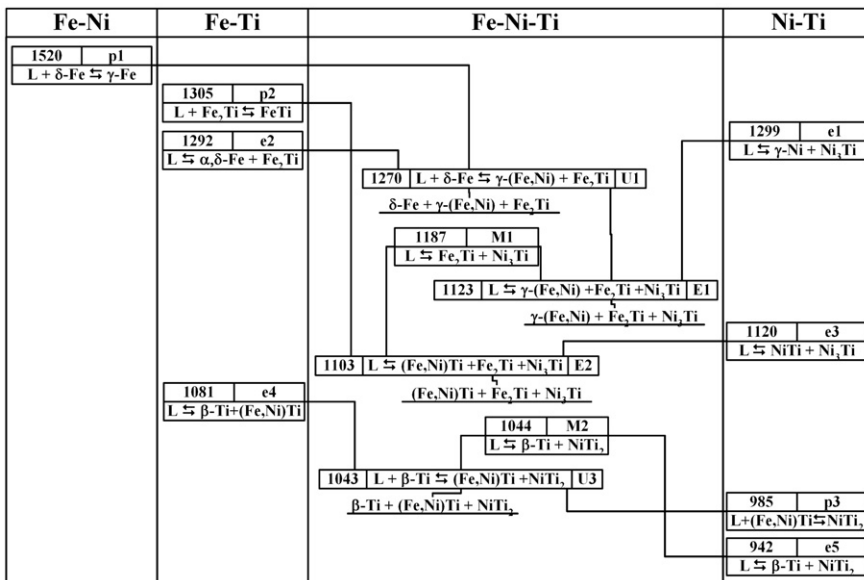


Fig. 25. Fe-Ni-Ti reaction scheme.

The Scheil diagram can also be calculated from the database (Fig. 25). It confirms the predicted reaction scheme from the critical assessment [1], except for the reaction $L + Fe_2Ti \rightarrow (Fe, Ni)Ti + Ni_3Ti$, which now appears as a eutectic reaction.

7. Conclusions

The Fe-Ni-Ti system was modeled following the CALPHAD method. The liquid phase was modeled using a regular solution model while all other phases were modeled using sublattice models. In particular 3 sublattices were used for the Laves phase, 2 for the ordered and disordered bcc and 4 for the fcc phases. Extrapolation from the binaries could provide a reasonable starting point considering the different phases that are in equilibrium with each other, but further optimization was necessary in order to obtain a good agreement with experimental phase boundaries and thermodynamic functions. The agreement with experiments is satisfactory. The optimization also confirms the critically assessed phase diagram of Cacciamani et al. [1].

Acknowledgements

This work has been carried out in the framework of the COST 535 "Thalu" project: the authors would like to acknowledge COST-ESF for supporting short scientific missions and meetings.

Appendix. Gibbs energy expressions

See Tables A.1–A.5.

References

- [1] G. Cacciamani, J. De Keyzer, R. Ferro, U.E. Klotz, J. Lacaze, P. Wollants, *Intermetallics* 14 (2006) 1312–1325.
- [2] R. Vogel, H.S. Wallbaum, *Arch. Eisenhüttenwes.* 12 (1938) 299–304.
- [3] N. Saunders, A.P. Miodownik, CALPHAD (Calculation of Phase Diagrams): A Comprehensive Guide, in: R.W. Cahn (Ed.), *Pergamon Materials Series*, vol. 1, Pergamon Press, Oxford, 1998.
- [4] H.L. Lukas, S.G. Fries, B. Sundman, *Computation Thermodynamics: The Calphad Method*, Cambridge University Press, 2007.
- [5] G. Inden, Project Meeting Calphad V, Dusseldorf: Max Plank Inst. Eisenforsch., 1976 (Chapter 3–4).
- [6] M. Hillert, M. Jarl, *CALPHAD* 2 (1978) 227–238.
- [7] M. Hillert, *J. Alloys Compounds* 320 (2001) 161–176.
- [8] I. Ansara, B. Sundman, P. Willemain, *Acta Metall.* 36 (1988) 977–982.
- [9] A. Kusoffsky, N. Dupin, B. Sundman, *CALPHAD* 25 (2001) 549–565.
- [10] N. Dupin, I. Ansara, *Z. Metall.* 90 (1999) 76–85.
- [11] A. Grytsiv, X.-Q. Chen, V.T. Witkiewicz, P. Rogl, R. Podloucky, V. Pomjakushin, D. Macciò, A. Saccone, G. Giester, F. Sommer, *Z. Kristallogr.* 221 (2006) 334–348.
- [12] K. Hagihara, T. Nakano, Y. Umakoshi, *Acta Metall.* 52 (2003) 2623–2637.
- [13] C.W. Yang, D.B. Williams, J.I. Goldstein, *J. Phase Equilib.* 17 (1996) 522–531.
- [14] F. Lechermann, M. Fhnle, J.M. Sanchez, *Intermetallics* 13 (2005) 1096–1109.
- [15] Y. Mishin, M.J. Mehl, D.A. Papaconstantopoulos, *Acta Metall.* 53 (2005) 4029–4041.
- [16] G. Cacciamani, A. Dinsdale, Personal communication.
- [17] R. Ruerand, E. Schuz, *Metallurgie* 7 (1910) 415–470.
- [18] D. Hanson, J.R. Freeman, *J. Iron Steel Inst.* 107 (1923) 301–321.
- [19] T. Kase, *Sci. Rep. Tohoku Imp. Univ.* 14 (1925) 173–217.
- [20] H. Bennedek, P. Schafmeister, *Arch. Eisenhüttenwes.* 5 (1931) 123–125.
- [21] C.H.M. Jenkins, E.H. Bucknall, C.R. Austin, G.A. Mellor, *J. Iron Steel Inst.* 136 (1937) 187–222.
- [22] E. Jossé, *Compt. Rend.* 230 (1950) 1467–1469.
- [23] A.H. Geisler, *Trans. ASM* 45 (1959) 1051–1054.
- [24] A. Hellawell, W. Hume-Rothery, *Philos. Trans. R. Soc. A-Math. Phys. Eng. Sci.* 249 (1957) 417–459.
- [25] T. Heumann, G. Karsten, *Arch. Eisenhüttenwes.* 34 (1963) 781–785.
- [26] J.I. Goldstein, R.E. Ogilvie, *Trans. Metall. Soc. AIME* 223 (1965) 2083–2087.
- [27] A.D. Romig, J.I. Goldstein, *Metall. Mater. Trans. A* 11 (1980) 1151–1159.
- [28] J.K. Van Deen, F. Van der Woude, *J. Phys.* 41 (C1) (1981) 367–368.
- [29] B. Predel, R. Mohs, *Arch. Eisenhüttenwes.* 41 (1970) 143–149.
- [30] G.I. Batalin, N.N. Mineko, V.S. Sundavtsova, *Russian Metall.* 5 (1974) 82–86.
- [31] Y. Iguchi, Y. Tozaki, M. Kakizaki, T. Fuwa, S. Ban-ya, *J. Iron Steel Inst. Jpn* 67 (1981) 925–932.
- [32] U. Thiedemann, M. Rösner-Kuhn, D.M. Matson, G. Kuppermann, K. Drewes, M.C. Flemings, M.G. Frohberg, *Steel Res.* 69 (1) (1998) 3–7.
- [33] B.J. Lee, *CALPHAD* 17 (1993) 251–168.
- [34] W. Steiner, O. Kriseisen, *Arch. Eisenhüttenwes.* 37 (1961) 701–707.
- [35] O. Kubaschewski, L.E.H. Stuart, *J. Chem. Eng. Data* 12 (1967) 418–420.
- [36] W.A. Dench, *Trans Faraday Soc.* 59 (1963) 1279–1292.
- [37] K.C. Hari Kumar, XXVIII CALPHAD meeting, Grenoble, May 2–7 1999.
- [38] J. Balun, Ph.D. Thesis, Access, Aachen, 2004.
- [39] J.L. Murray, *Phase Diagrams of Binary Titanium Alloys*, ASM Intl, Metals Park, OH, 1987, pp. 99–111.
- [40] C. Wagner, W. Schottky, *Z. Phys. Chemie-Int. J. Res. Phys. Chem.: Chem. Phys.* 11 (1930) 163–210.
- [41] A.D. McQuillan, *J. Inst. Met.* 79 (1951) 71.
- [42] H.W. Worner, *J. Inst. Met.* 79 (1951) 173.
- [43] R.J. Van Thyne, *Trans. ASM* 44 (1952) 974.
- [44] Y. Murakami, H. Kimura, Y. Nishimura, *Trans. Natl. Res. Inst. Met.* 1 (1959) 7.
- [45] G.R. Speich, *Trans. Metall. Soc. AIME* 224 (1962) 850.
- [46] N.G. Boriskina, I.I. Kornilov, Sb. Nouvye Titnov. Splanov, Moscow Izd. Nauk. 6 (1965) 61.
- [47] E.P. Abrahamson, S.L. Lopata, *Trans. Metall. Soc. AIME* 236 (1966) 76.
- [48] C. Booker, Ph.D. Thesis, Oregon graduate school, 1969.
- [49] M. Ko, T. Nishizawa, *J. Japan Inst. Met.* 43 (1979) 118–126.
- [50] J.K. Kivilahti, O.B. Tarasova, *Metall. Mater. Trans. A* 18 (1987) 1679–1680.
- [51] C.A. Qiu, Z.P. Jin, *Scripta Mater.* 28 (1993) 85–90.

- [52] J.L. Murray, in: P. Nash (Ed.), *Phase Diagrams of Binary Nickel Alloys*, ASM Intl., 1991, pp. 342–355.
- [53] R. Lück, B. Arpshofen, I. Predel, J.F. Smith, *Thermochim. Acta* 131 (1988) 171–181.
- [54] U. Thiedemann, M. Rsner-Kuhn, K. Drewes, G. Kuppermann, M.G. Frohberg, *J. Non-Cryst. Solids* 250 (1999) 329–335.
- [55] Y.O. Esin, M.G. Valishev, A.F. Ermakov, M.S. Petrushevskii, *Russ. J. Phys. Chem.* 55 (1981) 421–422.
- [56] P. Bellen, K.C. Hari Kumar, P. Wollants, *Z. Metall.* 87 (1996) 972–978.
- [57] W. Tang, B. Sundman, R. Sandström, C. Qiu, *Acta Mater.* 47 (1999) 3457–3468.
- [58] R. Vogel, H.S. Wallbaum, *Z. Metall.* 33 (1941) 376.
- [59] J.R. Long, E.T. Hayes, D.C. Root, C.E. Armentrout, *Bur. Mines RI* 4463 (1949).
- [60] A. Taylor, R.W. Floyd, *J. Inst. Met.* 80 (1951) 577–587.
- [61] H. Margolin, E. Ence, J.P. Nielsen, *Trans. AIME* 197 (1953) 243–247.
- [62] D.M. Poole, W. Hume-Rothery, *J. Inst. Met.* 83 (1954) 473–480.
- [63] Y.A Bagariatskii, Y.D. Tiapkin, *Soc. Phys. Cyrtallogr.* 2 (1957) 414–421.
- [64] E.R. Purdy, J. Gordon Parr, *Trans. AIME* 221 (1961) 636–639.
- [65] R.J. Wasilewski, S.R. Butler, J.E. Hanlon, D. Worden, *Metall. Trans.* 2 (1971) 229–238.
- [66] G.F. Bastin, G.D. Rieck, *Metall. Trans.* 5 (1974) 1817–1826.
- [67] C.C. Jia, K. Ishida, T. Nishizawa, *Met. Mat. Trans.* 25A (1994) 473–485.
- [68] J.C. Schuster, Z. Pan, S. Liu, F. Weitzer, Y. Du, *Intermetallics* 15 (2007) 1257–1267.
- [69] I. Ansara, Personal communication, 2001.
- [70] L.P. Dudkina, I.I. Kornilov, *Russ. Metall.* 4 (1967) 98–101.
- [71] F.J.J. Van Loo, J.W.G.A. Vrolifk, G.F. Bastin, *J. Less-Common Met.* 77 (1981) 121–130.
- [72] S.P. Alisova, P.B. Budberg, T.I. Barmina, N.V. Lutskaya, *Russ. Metall.* 1 (1994) 117–121.
- [73] N.L. Abramyccheva, *Vestnik Mosko. Univ. Ser. 2: Khimiya* 40 (1999) 139–143.
- [74] P. Riani, G. Cacciamani, Y. Thebaut, J. Lacaze, *Intermetallics* 14 (2006) 1226–1230.
- [75] G. Lück, H. Wang, B. Predel, *Z Metall.* 82 (1991) 805–809.
- [76] S.C. Drake, B.Sc. Thesis, MIT, 1982, p. 34.
- [77] SGTE pure element database ver. 4.4 updated from A.T. Dinsdale, CALPHAD 15 (1991) 317–425.
- [78] I. Ansara, Personal communication, 1995.
- [79] N. Dupin, B. Sundman, XXVII Jeep, *Journees d'Etude des Equilibre Entre Phases*, 2003.